

Aggregation and Deposition Kinetics of Fullerene (C₆₀) Nanoparticles

Kai Loon Chen and Menachem Elimelech*

Department of Chemical Engineering, Environmental Engineering Program, Yale University,
New Haven, Connecticut 06520-8286

Received July 17, 2006. In Final Form: September 10, 2006

The aggregation and deposition kinetics of fullerene C₆₀ nanoparticles have been investigated over a wide range of monovalent and divalent electrolyte concentrations by employing time-resolved dynamic light scattering (DLS) and quartz crystal microbalance (QCM), respectively. Aggregation kinetics of the fullerene nanoparticles exhibited reaction-limited (slow) and diffusion-limited (fast) regimes in the presence of both electrolytes, having critical coagulation concentrations (CCC) of 120 and 4.8 mM for the monovalent (NaCl) and divalent (CaCl₂) salts, respectively. The measured stability ratios of the aggregating fullerene nanoparticles were in very good agreement with Derjaguin–Landau–Verwey–Overbeek (DLVO) theory, with a derived Hamaker constant of 6.7×10^{-21} J for the fullerene nanoparticles in aqueous medium. For the deposition kinetics studies, the rate of fullerene nanoparticle deposition increased with increasing electrolyte concentrations, as was indicated in the aggregation kinetics results. However, at electrolyte concentrations approaching or exceeding the CCC, the rate of deposition dropped sharply due to significant concurrent aggregation of the fullerene nanoparticles. The deposition of the fullerene nanoparticles was further shown to be mostly irreversible, with immediate detachment of the nanoparticles observed only when exposed to a solution of high pH.

1. Introduction

Buckminsterfullerene C₆₀ has drawn immense attention in recent years for a variety of reasons. A landmark discovery,¹ C₆₀ has fascinated many with its spherical cage-like molecular structure. Furthermore, its discovery has led to the equally significant discovery of subsequent fullerenes, including carbon nanotubes.² Fullerene C₆₀ is undeniably living up to the promise of nanotechnology, with applications emerging in various fields, for instance, in the areas of biomedical technology,^{3,4} electronics,⁵ and optics.⁶

The major drawback of fullerene C₆₀ is that it has limited solubility in some organic solvents⁷ and is almost insoluble in water, thus restricting its potential methods of use.^{8–10} The nearest approximation to dissolving fullerene in water is to disperse it as nanoparticles. Several research groups have devised various techniques to synthesize fullerene nanoparticles suspended in water. One method is the solvent exchange technique which involves two steps: (1) dissolving fullerene in an organic solvent, such as tetrahydrofuran (THF) or toluene, and (2) introducing the mixture into water before removing the solvent through distillation or ultrasonication, and thus leaving the fullerene nanoparticles suspended in the aqueous phase.^{11,12} Another method involves simply stirring or ultrasonating the fullerene

in water over various periods of time.^{13–15} Ultraviolet–visible spectroscopy of fullerene nanoparticles that are synthesized through these two techniques reveals dissimilar profiles,^{13,16} indicating some disparity between the end products.

The mechanism of the nanoparticle synthesis is still unclear. However, it has been established that C₆₀ molecules tend to aggregate and self-assemble in different solvents.^{17–19} It is therefore reasonable to assume that the fullerene nanoparticle formation process involves the self-assembly of C₆₀ molecules. In fact, the mechanism of fullerene nanoparticle formation achieved by first dissolving fullerene in an organic solvent before mixing with water may be similar to the one in which both fullerene C₆₀ and C₇₀ molecules undergo aggregation in a binary solvent mixture comprising a weak and strong solvent.^{17,18} If that is the case, it is probable that the fullerene nanoparticles may contain voids within them, the presence of which is dependent upon the packing efficiency of the spherical molecules. Using static light scattering, Rudalevige et al.¹⁷ reported fractal dimensions of C₆₀ and C₇₀ aggregates in organic solvents of 2.9 and 2.1, respectively, thus confirming the presence of voids within the aggregate structures. Therefore, it is possible that solvent molecules such as water may be entrapped within the voids of fullerene nanoparticles.

An intriguing observation is that the supposedly purely carbon-based fullerene nanoparticles have a negative electrophoretic

* Corresponding author. E-mail: menachem.elimelech@yale.edu. Phone: (203) 432-2789.

(1) Kroto, H. W.; Heath, J. R.; O'Brien, S. C.; Curl, R. F.; Smalley, R. E. *Nature* **1985**, *318* (6042), 162–163.

(2) Iijima, S. *Nature* **1991**, *354* (6348), 56–58.

(3) Zakharian, T. Y.; Seryshev, A.; Sitharaman, B.; Gilbert, B. E.; Knight, V.; Wilson, L. J. *J. Am. Chem. Soc.* **2005**, *127* (36), 12508–12509.

(4) Noon, W. H.; Kong, Y. F.; Ma, J. P. *Proc. Natl. Acad. Sci. U.S.A.* **2002**, *99*, 6466–6470.

(5) King, R. B. *J. Chem. Inf. Comp. Sci.* **1999**, *39* (2), 180–191.

(6) Sun, Y. P.; Riggs, J. E.; Liu, B. *Chem. Mater.* **1997**, *9* (5), 1268–1272.

(7) Ruoff, R. S.; Tse, D. S.; Malhotra, R.; Lorents, D. C. *J. Phys. Chem.* **1993**, *97* (13), 3379–3383.

(8) Ying, Q. C.; Zhang, J.; Liang, D. H.; Nakanishi, W.; Isobe, H.; Nakamura, E.; Chu, B. *Langmuir* **2005**, *21* (22), 9824–9831.

(9) Alargova, R. G.; Deguchi, S.; Tsujii, K. *J. Am. Chem. Soc.* **2001**, *123* (43), 10460–10467.

(10) Li, H. G.; Jia, X. F.; Li, Y.; Shi, X. W.; Hao, J. C. *J. Phys. Chem. B* **2006**, *110* (1), 68–74.

(11) Andrievsky, G. V.; Kosevich, M. V.; Vovk, O. M.; Shelkovsky, V. S.; Vashchenko, L. A. *J. Chem. Soc. Chem. Commun.* **1995**, *12*, 1281–1282.

(12) Deguchi, S.; Alargova, R. G.; Tsujii, K. *Langmuir* **2001**, *17* (19), 6013–6017.

(13) Brant, J.; Lecoanet, H.; Hotze, M.; Wiesner, M. *Environ. Sci. Technol.* **2005**, *39* (17), 6343–6351.

(14) Jakubczyk, D.; Derkachov, G.; Bazhan, W.; Lusakowska, E.; Kolwas, K.; Kolwas, M. *J. Phys. (Paris) D Appl. Phys.* **2004**, *37* (20), 2918–2924.

(15) Deguchi, S.; Mukai, S.; Tsudome, M.; Horikoshi, K. *Adv. Mater.* **2006**, *18* (6), 729–732.

(16) Mchedlov-Petrosyan, N. O.; Klochkov, V. K.; Andrievsky, G. V. *J. Chem. Soc., Faraday Trans.* **1997**, *93* (24), 4343–4346.

(17) Rudalevige, T.; Francis, A. H.; Zand, R. *J. Phys. Chem. A* **1998**, *102* (48), 9797–9802.

(18) Sun, Y. P.; Ma, B.; Bunker, C. E.; Liu, B. *J. Am. Chem. Soc.* **1995**, *117* (51), 12705–12711.

(19) Nath, S.; Pal, H.; Palit, D. K.; Sapre, A. V.; Mittal, J. P. *J. Phys. Chem. B* **1998**, *102* (50), 10158–10164.

mobility or zeta potential, regardless of the synthesis techniques described previously.^{12,13,16} Brant et al.²⁰ recently verified the negative electrophoretic mobility of fullerene nanoparticles synthesized through three solvent exchange methods while employing different combinations of solvents, as well as by the method that consists of the extended mixing of fullerene with water. Although some discussion has occurred and hypotheses have been made,¹³ the origin of the negative zeta potential (or surface charge) still has yet to be ascertained.

Due to the surface charge property of fullerene nanoparticles, it is of interest to know if the classic Derjaguin–Landau–Verwey–Overbeek (DLVO) theory^{21,22} can adequately describe the stability to aggregation and deposition of these engineered nanoparticles. It has been suggested that this is likely,^{12,16,23,24} but no rigorous studies have been conducted to quantitatively establish the aggregation and deposition kinetics as functions of electrolyte concentrations. It is imperative to quantitatively understand the aggregation behavior of fullerene nanoparticles in order to better utilize them for potential applications.¹²

Currently, fullerene is already being employed in the manufacturing of some consumer products, such as cosmetics.²⁵ With the anticipated widespread manufacture and use of fullerene-based products occurring soon,²⁶ it is inevitable that some of the fullerene may be released into the natural environment as contaminants. If they were to be introduced into natural aquatic systems, either in bulk form or dissolved in organic solvents, it is likely that they would end up as nanoparticles due to extended mixing that would occur naturally as they are transported within the systems. With the emergence of nanotechnology, the concern over the effects of possible toxicity of nanomaterials on humans, as well as their impacts on the environment and ecology, is growing.^{27–32} Recently, several studies have highlighted the toxicity of fullerene nanoparticles on microbes,²⁶ fish,³³ and human cells.^{34,35} On the other hand, there are also studies and reports which have indicated otherwise.^{36,37} Nevertheless, the concern is indisputably mounting.

Once released into natural aquatic systems, the bioavailability of the fullerene nanoparticles is directly determined by their fate and transport within these systems. The propensity of these nanoparticles to aggregate will govern their aggregate size and

compactness, thus influencing their settling rate and eventual removal from the aquatic phase. Also, nanoparticles may interact with and attach to mineral surfaces, leading to the depletion of these nanoparticles from solution. On occasions when the solution chemistry of the natural waters changes significantly, for instance after a rainfall, deposited fullerene nanoparticles may be released from the mineral surfaces and reenter the aquatic environment.

While the mechanism of the apparent toxicity of fullerene nanoparticles is still being debated,³⁸ the aggregation state of the nanoparticles may perhaps play a role in determining its level of toxicity. Aggregation of the nanoparticles may lead to significantly large aggregates, such that the partition of the aggregates into cell membranes or their transport through the human or animal body, both possible mechanisms for engineered nanomaterial toxicity suggested by Oberdörster,³³ may be impeded. However, these mechanisms are yet to be verified in the case of fullerene nanoparticles.

The objective of this paper is to quantify and compare the aggregation and deposition kinetics of fullerene nanoparticles in common monovalent and divalent electrolyte solutions. The aggregation kinetics of the nanoparticles were derived by employing time-resolved dynamic light scattering (DLS) over a range of electrolyte concentrations. Deposition kinetics of the fullerene nanoparticles onto a silica surface were determined using the quartz crystal microbalance (QCM). Both the fullerene deposition and aggregation behaviors were found to be in good agreement with the classic DLVO theory for colloidal stability. Deposition of the fullerene nanoparticles was mostly irreversible, whereby release of the nanoparticles was only observed at high solution pH.

2. Materials and Methods

2.1. Fullerene Nanoparticle Synthesis and Characterization.

The fullerene nanoparticles were synthesized through the method described by Andrievsky et al.¹¹ About 36 mg of 99.9% pure C₆₀ powder (MER Corporation, Tucson, AZ) was dissolved in 30 mL of HPLC-grade toluene (Sigma-Aldrich, St. Louis, MO) by stirring for a few hours, resulting in a clear dark purple mixture. A total of 5 mL of this mixture was gently introduced into a solution of 50 mL of deionized water (Barnstead) and 1.5 mL of HPLC-grade ethanol (Sigma-Aldrich, St. Louis, MO), forming two distinct phases. The mixture was sonicated with a sonicating probe (450 Sonifier, Branson Ultrasonics Corporation, Danbury, CT) in a fume hood for more than 3 h to allow for the evaporation of toluene and ethanol. Throughout this sonication process, the mixture was topped off with deionized water every 20 min to compensate for water loss through evaporation. The final solution was filtered under vacuum, first through a 0.45 μm membrane filter followed by a 0.2 μm membrane filter (Fisher Scientific). According to the manufacturer, both membrane filters are made of a mixture of cellulose acetate and cellulose nitrate. The resulting clear yellow filtrate containing the fullerene nanoparticles was collected and stored in the dark at 4 °C. Five such batches were synthesized and combined to form about 250 mL of fullerene nanoparticle stock suspension. Through high-temperature oxidation at 680 °C (TOC–V CSH, Shimadzu, Kyoto, Japan), we determined the fullerene nanoparticle stock suspension to have a total carbon content of 5.92 mg/L. All aggregation, deposition, and release experiments were completed within 2 months after the synthesis of the nanoparticles.

In preparation for transmission electron microscope (TEM) examination, the fullerene nanoparticles were adsorbed onto nickel grids by leaving each grid on a drop of fullerene nanoparticle stock suspension for 5 min. The nanoparticles were then observed under a Tecnai 12 Biotwin electron microscope (FEI Company, Hillsboro, OR) at 100 kV. TEM images of the nanoparticles were captured digitally for further size analysis.

(20) Brant, J. A.; Labille, J.; Bottero, J. Y.; Wiesner, M. R. *Langmuir* **2006**, *22* (8), 3878–3885.

(21) Derjaguin, B. V.; Landau, L. D. *Acta Physicochim. URSS* **1941**, *14*, 733–762.

(22) Verwey, E. J. W.; Overbeek, J. T. G. *Theory of the Stability of Lyophobic Colloids*; Elsevier: Amsterdam, 1948.

(23) Brant, J.; Lecoanet, H.; Wiesner, M. R. *J. Nanopart. Res.* **2005**, *7* (4–5), 545–553.

(24) Lecoanet, H. F.; Wiesner, M. R. *Environ. Sci. Technol.* **2004**, *38* (16), 4377–4382.

(25) Halford, B. *Chem. Eng. News* **2006**, *84* (13), 47–47.

(26) Fortner, J. D.; Lyon, D. Y.; Sayes, C. M.; Boyd, A. M.; Falkner, J. C.; Hotze, E. M.; Alemany, L. B.; Tao, Y. J.; Guo, W.; Ausman, K. D.; Colvin, V. L.; Hughes, J. B. *Environ. Sci. Technol.* **2005**, *39* (11), 4307–4316.

(27) Masciangioli, T.; Zhang, W. X. *Environ. Sci. Technol.* **2003**, *37* (5), 102a–108a.

(28) Roco, M. C. *Environ. Sci. Technol.* **2005**, *39* (5), 106a–112a.

(29) Nel, A.; Xia, T.; Madler, L.; Li, N. *Science* **2006**, *311* (5761), 622–627.

(30) Colvin, V. L. *Nat. Biotechnol.* **2003**, *21* (10), 1166–1170.

(31) Dreher, K. L. *Toxicol. Sci.* **2004**, *77* (1), 3–5.

(32) Wiesner, M. R.; Lowry, G. V.; Alvarez, P.; Dionysiou, D.; Biswas, P. *Environ. Sci. Technol.* **2006**, *40* (14), 4336–4345.

(33) Oberdörster, E. *Environ. Health Perspect.* **2004**, *112* (10), 1058–1062.

(34) Sayes, C. M.; Fortner, J. D.; Guo, W.; Lyon, D.; Boyd, A. M.; Ausman, K. D.; Tao, Y. J.; Sitharaman, B.; Wilson, L. J.; Hughes, J. B.; West, J. L.; Colvin, V. L. *Nano Lett.* **2004**, *4* (10), 1881–1887.

(35) Sayes, C. M.; Gobin, A. M.; Ausman, K. D.; Mendez, J.; West, J. L.; Colvin, V. L. *Biomaterials* **2005**, *26* (36), 7587–7595.

(36) Gharbi, N.; Pressac, M.; Hadchouel, M.; Szwarc, H.; Wilson, S. R.; Moussa, F. *Nano Lett.* **2005**, *5* (12), 2578–2585.

(37) Andrievsky, G.; Klochkov, V.; Derevyanchenko, L. *Fuller Nanotube Carbon* **2005**, *13* (4), 363–376.

(38) Lyon, D. Y.; Adams, L. K.; Falkner, J. C.; Alvarez, P. J. J. *Environ. Sci. Technol.* **2006**, *40* (14), 4360–4366.

The electrophoretic mobilities of the nanoparticles were measured over a range of NaCl and CaCl₂ concentrations (ZetaPALS, Brookhaven Instruments Corp., Holtsville, NY) at pH 5.2 and 25 °C. For each solution condition, 10 measurements were conducted for each of at least 3 samples.

2.2. Solution Chemistry. The electrolyte (NaCl and CaCl₂) stock solutions were prepared and filtered through 0.1 μm filters (Anotop 25, Whatman, Middlesex, U.K.) before use. All experiments and measurements were conducted at pH 5.2 ± 0.1, at which the fullerene nanoparticles are stable at low ionic strengths.

2.3. Dynamic Light Scattering. The DLS measurements were performed with a multi-detector light scattering unit (ALV-5000, Langen, Germany) which employs a Nd:vanadate laser (Verdi V2, Coherent, Santa Clara, CA) with a wavelength of 532 nm. The fullerene nanoparticle stock solution was diluted 20 times with deionized water for the DLS experiments. For each experiment, 2 mL of the diluted suspension was introduced into a glass vial (Supelco, Bellefonte, PA) which had been soaked in cleaning solution (Extran MA01, Merck KGaA, Darmstadt, Germany), thoroughly rinsed with deionized water, and oven-dried under dust-free conditions. All vials were used only once. A premeasured amount of electrolyte stock solution was introduced into the vial containing the diluted nanoparticle suspension to induce aggregation. The vial was briefly vortexed (Mini Vortexer, Fisher Scientific) before being inserted into the toluene-filled quartz vat of the light scattering unit, and the DLS measurements were started immediately. The scattered light intensity was detected by a photodetector at a scattering angle of 90°, and each auto-correlation function was accumulated for 15 s. The intensity-weighted hydrodynamic radius of the aggregates was determined through second-order cumulant analysis (ALV software). The nanoparticle samples were left to aggregate for between 20 min and 2.5 h to allow for an increase in the intensity-weighted hydrodynamic radius of at least 25% of the initial hydrodynamic radius of the suspension, a_{h0} . This initial increase in the hydrodynamic radius was usually linear with respect to time. However, for aggregation at low salt concentrations, the initial increase in the hydrodynamic radius ceased to be linear with respect to time before reaching 1.25 a_{h0} . All DLS measurements were conducted at 23 °C.

2.4. Determination of Nanoparticle Aggregation Kinetics. The early-stage aggregation kinetics are expressed as the initial rate of increase in the hydrodynamic radius $a_h(t)$ with time t , as measured by DLS. This increase in $a_h(t)$ is linearly dependent on the initial (primary) particle concentration, N_0 , as well as the initial aggregation rate constant, k_{11} ^{39–41}

$$\left(\frac{da_h(t)}{dt}\right)_{t \rightarrow 0} \propto k_{11}N_0 \quad (1)$$

The initial rate of increase in $a_h(t)$ is obtained through a consistent approach by determining the initial slope up to the point where the hydrodynamic radius reaches 1.25 a_{h0} . When very low electrolyte concentrations are employed to induce aggregation, the linear regime usually ends before reaching 1.25 a_{h0} . Under such scenarios, the slope of the linear regime is determined even if it ends before 1.25 a_{h0} . For all cases, we always verified that the fitted line intercepts the y axis no more than 3 nm in excess of a_{h0} .

From eq 1, the aggregation attachment efficiencies α_A (otherwise known as the inverse stability ratio, $1/W$) at different electrolyte concentrations are then calculated by normalizing the slopes obtained under the different solution conditions by the slope obtained under “favorable” (fast) aggregation conditions

$$\alpha_A = \frac{1}{W} = \frac{k_{11}}{(k_{11})_{\text{fast}}} = \frac{\frac{1}{N_0} \left(\frac{da_h(t)}{dt}\right)_{t \rightarrow 0}}{\frac{1}{(N_0)_{\text{fast}}} \left(\frac{da_h(t)}{dt}\right)_{t \rightarrow 0, \text{fast}}} \quad (2)$$

Here, the terms with subscript “fast” refer to favorable (nonrepulsive) aggregation conditions. It is necessary to account for the initial particle concentrations in eq 2 since different volumes of electrolyte stock

solution were introduced into the 2 mL of the diluted nanoparticle suspension for different aggregation experiments. The aggregation attachment efficiency, α_A , ranging from 0 to 1, serves to quantify the initial aggregation kinetics of the fullerene nanoparticles in different electrolyte concentrations.

2.5. Quartz Crystal Microbalance. A quartz crystal microbalance with dissipation monitoring (QCM-D) was employed to measure the deposition kinetics of fullerene nanoparticles onto the silica-coated quartz surface. The QCM-D unit E4 (Q-Sense AB, Västra Frölunda, Sweden) comprises a measurement chamber platform which mounts 4 sensor flow modules. Each flow module holds a 5 MHz AT-cut quartz sensor crystal with a silica-coated surface. The crystals were presoaked in 2% Hellmanex II (Hellma GmbH & Co. KG, Müllheim, Germany) cleaning solution overnight, thoroughly rinsed with deionized water, and oxidized for 20 min in a UV-ozone chamber. We verified the quality of the crystals prepared according to this cleaning protocol before each experiment by ensuring that the measured QCM-D dissipation values in deionized water were within the allowable range.

The flow modules in the QCM-D are arranged in a parallel flow configuration, which allowed the test solution to be driven across the four crystal surfaces within the modules simultaneously using a peristaltic pump. We employed two or three of the four modules to obtain adequate replicates of the deposition experiment for each electrolyte concentration. The fullerene nanoparticle stock suspension was diluted 2 times for all the deposition experiments in order to achieve a sufficient degree of attachment onto the silica surface across a range of electrolyte concentrations. Both the prepared electrolyte solutions and diluted fullerene nanoparticle suspension were sonicated for about 15 min in order to degas the solutions and thus prevent air bubble formation in the E4 system during the deposition experiments. The solutions were subsequently stored in a water bath at a temperature of 27 °C, 2 °C above the temperature employed for the deposition experiments.

The electrolyte solution, having the concentration at which deposition was to be conducted, was first flowed across the silica surface until the normalized frequency at the third overtone stabilized. For deposition experiments with low deposition rates, we ensured that the average normalized frequency ceased to drift more than 0.2 Hz in a time period of 1 h. Once a stable baseline was achieved, a premeasured volume of electrolyte stock solution was introduced into the diluted fullerene nanoparticle suspension immediately prior to the deposition experiment to obtain the desired electrolyte concentration. The suspension was then flowed through the QCM-D modules. As deposition of the fullerene nanoparticles on the silica surface took place, the continuous increase in the mass of the crystal due to the deposited nanoparticles induced a continuous shift in the resonance and overtone frequencies, as described by the Sauerbrey relationship⁴²

$$\Delta m = -\frac{C\Delta f_n}{n} \quad (3)$$

where Δm is the mass of fullerene nanoparticles deposited, Δf_n is the shift in resonance (or overtone) frequency, with n being the overtone number (1, 3, 5, and 7), and C is the crystal constant (17.7 ng/Hz·cm² for the 5 MHz quartz crystal).

For all of the deposition experiments, the flow rate through each module was 0.1 mL/min (±0.002 mL/min), and the temperature within the modules was maintained at 25 °C. According to the manufacturer, such a flow rate results in laminar flow through each flow module. Time periods between 20 and 60 min were provided to allow sufficient deposition for determining the nanoparticle deposition rate.

(39) Chen, K. L.; Mylon, S. E.; Elimelech, M. *Environ. Sci. Technol.* **2006**, *40* (5), 1516–1523.

(40) Holthoff, H.; Egelhaaf, S. U.; Borkovec, M.; Schurtenberger, P.; Sticher, H. *Langmuir* **1996**, *12* (23), 5541–5549.

(41) Mylon, S. E.; Chen, K. L.; Elimelech, M. *Langmuir* **2004**, *20* (21), 9000–9006.

(42) Sauerbrey, G. *Z. Phys.* **1959**, *155* (2), 206–222.

2.6. Determination of Nanoparticle Deposition Kinetics. Since the changes in resonance and overtone frequencies are proportional to the mass deposited on the crystal, the rate of deposition is indicated by the rate of frequency shift. In our study, we monitored the normalized frequency shift at the third overtone ($\Delta f_{(3)} = \Delta f_3/3$) to determine the deposition rate at different electrolyte concentrations. The deposition attachment efficiency, α_D , is used to quantify the deposition kinetics at different electrolyte concentrations

$$\alpha_D = \frac{d\Delta f_{(3)}/dt}{(d\Delta f_{(3)}/dt)_{\text{fav}}} \quad (4)$$

Here, the numerator and denominator terms represent the rates of shift in the normalized frequency at the electrolyte concentration studied and under fast, favorable deposition conditions, respectively. The latter has been determined experimentally as described below.

Because both the silica surface and fullerene nanoparticles are negatively charged at the studied solution conditions (pH 5.2), favorable (nonrepulsive) deposition conditions were induced by modifying the silica surface, which involved precoating it with a layer of positively charged poly-L-lysine (PLL) polyelectrolyte (P-1274, Sigma-Aldrich, St. Louis, MO). The PLL (93 800 Da) was prepared in a solution made up of 10 mM *N*-(2-hydroxyethyl)-piperazine-*N'*-(2-ethanesulfonic acid) (HEPES, H4034-100G, Sigma-Aldrich, St. Louis, MO) and 100 mM NaCl filtered through a 0.22 μm cellulose acetate filter. The crystals were first equilibrated by flowing the PLL-free solution (10 mM HEPES and 100 mM NaCl) at 0.1 mL/min across the substrate surface until the normalized frequency at the third overtone attained a constant value. Next, the PLL solution was flowed across the silica surface until no change in the normalized frequency was observed, indicating that the silica surface had been fully coated with PLL. A 1 mM NaCl solution was flowed through the modules to remove the unadsorbed PLL, and the fullerene nanoparticles were then deposited onto the PLL-coated surface in a 1 mM NaCl solution. The rate of shift in the normalized frequency under this favorable deposition condition was measured to be 1.157 Hz/min (± 0.031 Hz/min) as obtained from three deposition experiments. From eq 3, this value corresponds to a fullerene mass deposition rate of 20.5 ng/min \cdot cm².

3. Results and Discussion

3.1. Characteristics of Fullerene Nanoparticles. TEM imaging of the fullerene nanoparticles (Figure 1a) shows that they are polydisperse and mainly spherical with slight angular features. Since the nanoparticles are not electron-dense, they appeared translucent under the TEM. Occasionally, it was possible to observe parallel planes within the nanoparticles, which may imply that the nanoparticles have a crystalline structure. This observation may be dependent on the orientation of the nanoparticles adsorbed on the grid.

To describe the size distribution, fullerene nanoparticles were adsorbed onto 3 TEM grids as discussed in the previous section. The diameters (or longest dimensions for slightly elongated nanoparticles) for 360 nanoparticles were determined from the TEM images of the nanoparticles as analyzed by ImageJ software (National Institutes of Health). To avoid bias, all observed nanoparticles on the three TEM grids were measured. Figure 1b shows the size distribution of the 360 nanoparticles, with each bar representing a diameter range of 10 nm. The number-average diameter (or longest dimension) is 59.2 nm, with a standard deviation of 22.7 nm. About 94% of the nanoparticles have longest dimensions smaller than 100 nm.

The intensity-weighted hydrodynamic radius of the freshly synthesized fullerene nanoparticles, a_{h0} , was measured to be 55.7 nm (± 1.8 nm) based on 20 DLS measurements. This value is reasonable since the scattered light intensity of a particle is

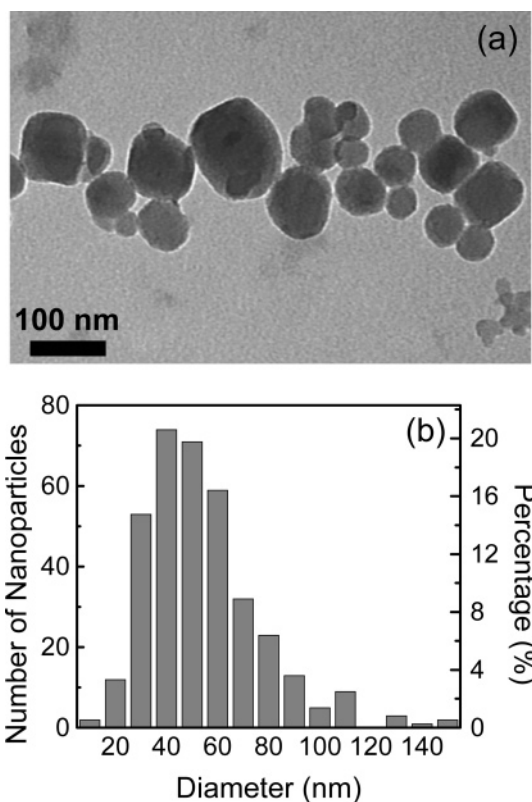


Figure 1. (a) TEM image of fullerene nanoparticles. (b) Size distribution of 360 fullerene nanoparticles adsorbed on three TEM grids. Longest dimensions are measured for slightly elongated particles. Each bar represents a diameter range of 10 nm.

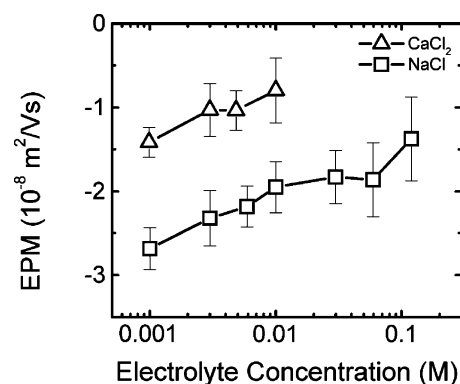


Figure 2. Electrophoretic mobilities (EPM) of fullerene nanoparticles as functions of NaCl and CaCl₂ concentrations at pH 5.2. Each data point represents the mean of at least a total of 30 measurements of at least three different samples at each electrolyte concentration, and the error bars represent standard deviations. Measurements were conducted at 25 °C.

proportional to the square of its volume within the limits of the Rayleigh–Gans–Debye approximation.⁴⁰ We verified that there was no significant change in the hydrodynamic radius 2 months after the nanoparticle synthesis. After 6 months, we noted that the hydrodynamic radius increased slightly to 58.2 nm (± 1.5 nm), indicating the occurrence of slow aggregation in the fullerene nanoparticle stock suspension over a prolonged period of time.

The electrophoretic mobilities of the fullerene nanoparticles as a function of salt concentration are shown in Figure 2. Although the fullerene nanoparticles exhibit negatively charged surfaces, the mechanism by which the nanoparticles acquire a negative surface charge is still unclear. As discussed earlier in the paper, other studies also reported that fullerene nanoparticles synthesized

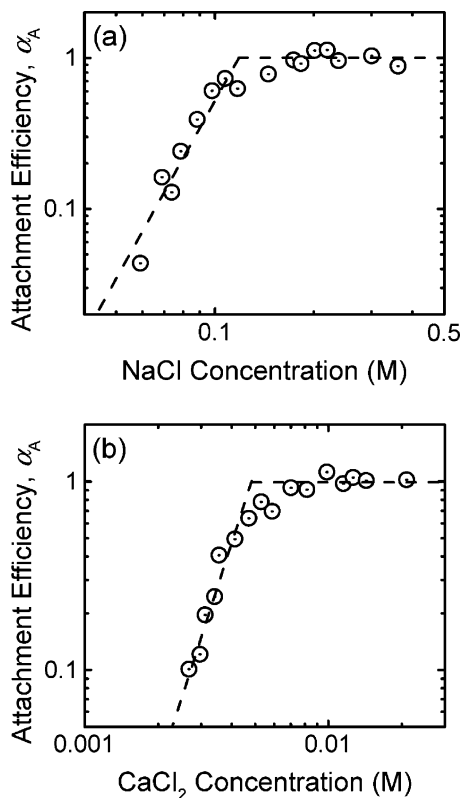


Figure 3. (a) Attachment efficiencies (or inverse stability ratios, $1/W$) of fullerene nanoparticles as a function of NaCl concentration at pH 5.2. The CCC based on these data is 120 mM NaCl. (b) Attachment efficiencies (or inverse stability ratios, $1/W$) of fullerene nanoparticles as a function of CaCl₂ concentration at pH 5.2. The CCC based on these data is 4.8 mM CaCl₂. The lines (used as eye guides) are extrapolated from the reaction-limited and diffusion-limited regimes, and their intersections yield the respective CCC.

by this technique, as well as by other techniques, have a net negative surface charge.^{12,16,20} For both NaCl and CaCl₂, as the electrolyte concentration was increased, the electrophoretic mobility of the fullerene nanoparticles became less negative, as is commonly observed with most colloidal particles in aqueous solutions. Also, Ca²⁺ was much more effective in reducing the electrophoretic mobility of the fullerene nanoparticles than Na⁺, which may be indicative of specific adsorption of calcium ions to the nanoparticle surface.⁴³

3.2. Aggregation Kinetics with Sodium and Calcium Cations. The aggregation of the fullerene nanoparticles has been studied over NaCl concentrations ranging from 59 to 362 mM and CaCl₂ concentrations ranging from 2 to 21 mM at pH 5.2. The aggregation attachment efficiencies as functions of NaCl and CaCl₂ concentrations are presented in Figure 3. By taking the initial slopes of the aggregation profiles and accounting for the initial particle concentrations as described in eq 2, it was verified that the average $(k_{11})_{\text{fast}}$ values obtained at high NaCl and CaCl₂ concentrations are the same, thereby confirming that aggregation kinetics are diffusion-controlled under such conditions. Distinct reaction-limited (slow) and diffusion-limited (fast) aggregation regimes⁴⁴ are observed for the fullerene nanoparticles in the presence of both NaCl and CaCl₂. This observation indicates that the aggregation behavior of the fullerene nanoparticles is in

general agreement with the DLVO theory. This is also consistent with our earlier observation that, with an increase in either electrolyte concentration, the nanoparticles become less negatively charged, even though we are still uncertain about the origin of the nanoparticle surface charge.

In the reaction-limited regime, an increase in the electrolyte concentration screens the surface charge of the nanoparticles, and reduces the energy barrier to aggregation, thus leading to faster aggregation. However, at the critical coagulation concentration (CCC), and at electrolyte concentrations above the CCC, the energy barrier is eliminated, leading to diffusion-controlled aggregation (i.e., $\alpha_A = 1/W = 1$). The intersections between the extrapolations through the reaction- and diffusion-limited regimes yield the CCC in the respective electrolytes. Based on our data, we determine the CCC to be 120 mM for NaCl and 4.8 mM for CaCl₂. Our CCC in NaCl is higher than that derived through turbidity tests by Mchedlov-Petrosyan et al.¹⁶ (85 mM) for fullerene nanoparticles synthesized by the same technique. Their reported CCC in CaCl₂ is 4.1 mM, which is close to our obtained value. The ratio of CCC values we derived (4.8/120) is proportional to $z^{-4.64}$, where z is the valence of the calcium counterion (i.e., $z = 2$). This is reasonable as the Schulze–Hardy rule predicts a proportionality to z^{-6} for particles of large zeta potentials, whereas it has also been reported that a much weaker dependence on the counterion charge (z^{-2}) exists for particles with small zeta potentials.⁴³

3.3. Comparison to DLVO Prediction. The stability ratio of aggregating nanoparticles with the inclusion of colloidal and hydrodynamic interactions is given by⁴⁵

$$W = \frac{\int_0^{\infty} \beta(h) \frac{\exp[V_T(h)/kT] dh}{(2a+h)^2}}{\int_0^{\infty} \beta(h) \frac{\exp[V_A(h)/kT] dh}{(2a+h)^2}} \quad (5)$$

where h is the surface-to-surface separation distance between two particles, a is the particle radius, k is the Boltzmann constant, and T is the absolute temperature. Because of the polydispersity of the fullerene nanoparticles, a was taken to be 29.6 nm, namely, half of the number-average diameter of 59.2 nm. The total interaction energy between two particles, $V_T(h)$, is the sum of the van der Waals attraction, $V_A(h)$, and electrical double layer interaction. The dimensionless function $\beta(h)$ corrects for the hydrodynamic resistance (interaction) between the two approaching particles⁴⁶

$$\beta(h) = \frac{6\left(\frac{h}{a}\right)^2 + 13\left(\frac{h}{a}\right) + 2}{6\left(\frac{h}{a}\right)^2 + 4\left(\frac{h}{a}\right)} \quad (6)$$

The van der Waals attraction, $V_A(h)$, was calculated by the expression proposed by Gregory⁴⁷ that accounts for the electromagnetic retardation effect. Because the origin of surface charge of the fullerene nanoparticles is not well understood, the linear superposition approximation (LSA) expression⁴⁸ was used to calculate the electrical double layer interaction. This expression does not make any assumption regarding the potential or charge

(43) Elimelech, M.; Gregory, J.; Jia, X.; Williams, R. A. *Particle Deposition and Aggregation: Measurement, Modelling and Simulation*; Butterworth-Heinemann: Oxford, U.K., 1995.

(44) Weitz, D. A.; Huang, J. S.; Lin, M. Y.; Sung, J. *Phys. Rev. Lett.* **1985**, *54* (13), 1416–1419.

(45) McGown, D. N. L.; Parfitt, G. D. *J. Phys. Chem.* **1967**, *71* (2), 449–450.

(46) Honig, E. P.; Roebse, G.; Wiersema, P. H. *J. Colloid Interface Sci.* **1971**, *36* (1), 97–109.

(47) Gregory, J. *J. Colloid Interface Sci.* **1981**, *83* (1), 138–145.

(48) Gregory, J. *J. Colloid Interface Sci.* **1975**, *51* (1), 44–51.

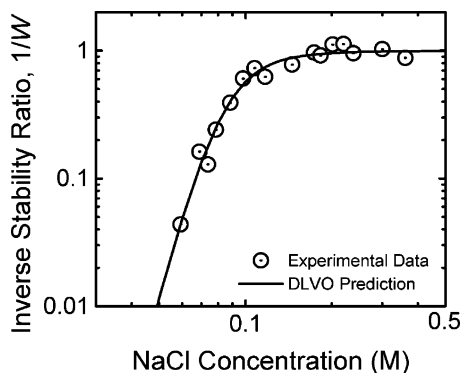


Figure 4. Theoretical DLVO prediction and experimentally derived inverse stability ratios (or aggregation attachment efficiencies, α_A) of fullerene nanoparticles as a function of NaCl concentration at pH 5.2. The experimentally derived inverse stability ratios are the same as those presented in Figure 3a. The Hamaker constant of fullerene nanoparticles in aqueous medium, A_{FWF} , employed for the theoretical prediction is 6.7×10^{-21} J.

at the particle surface and gives intermediate results between the two extremes of constant surface potential⁴⁹ and constant surface charge^{50,51} expressions.

Using eqs 5 and 6, we fitted the experimentally derived inverse stability ratios $1/W$ (or aggregation attachment efficiencies α_A) over a range of NaCl concentrations (presented earlier in Figure 3a) with the theoretically predicted $1/W$ profile. In this procedure, we used the fullerene nanoparticle Hamaker constant, A_{FWF} , which is required by the expression for $V_A(h)$,⁴⁷ as the only fitting parameter. In the process, we converted the average electrophoretic mobilities of the fullerene nanoparticles at different NaCl concentrations (presented previously in Figure 2) to ζ potentials using the tabulated values provided by Ottewill and Shaw.⁵²

The theoretical stability curve (i.e., the logarithm of $1/W$ versus the logarithm of molar NaCl concentration) is compared to the experimental data in Figure 4. The Hamaker constant, A_{FWF} , needed to fit the experimental data was 6.7×10^{-21} J. The results show a remarkable agreement between DLVO predictions and experimental data, which is quite rare in studies of aggregation kinetics of colloidal particles under conditions where repulsive electrostatic interactions predominate.^{43,50,53} In such past aggregation studies, the predicted slopes of the stability curves based on DLVO theory are much steeper than those obtained experimentally.^{43,54,55}

As discussed previously, the fullerene nanoparticles are formed through the aggregation/crystallization of C₆₀ molecules and thus possibly contain voids within the nanoparticles, depending on the packing density. Our derived Hamaker constant is the effective Hamaker constant of the fullerene nanoparticles that contain water within the voids. The Hamaker constant of bulk fullerene materials in water, like C₆₀ or carbon nanotubes, should be greater than 6.7×10^{-21} J. For comparison, our derived Hamaker constant for the fullerene nanoparticles in water ($A_{FWF} = 6.7 \times 10^{-21}$ J) is even smaller than the reported value for polystyrene latex particles in aqueous media (9.5×10^{-21} J).⁵³

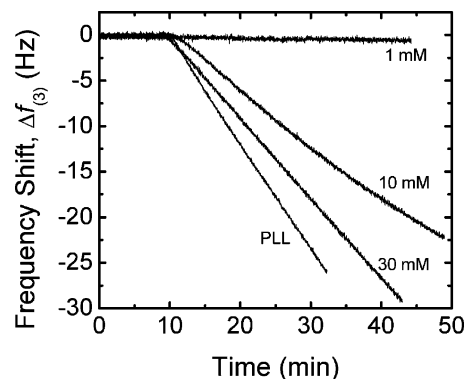


Figure 5. Deposition of fullerene nanoparticles onto a silica-coated quartz surface indicated by normalized frequency shifts at the third overtone in the presence of 1, 10, and 30 mM NaCl at pH 5.2. Favorable deposition rate (shown as “PLL”) is obtained by coating the silica surface with positively charged poly-L-lysine (PLL), prior to conducting the deposition experiment in the presence of 1 mM NaCl at pH 5.2.

By employing the relationship^{43,56}

$$A_{FWF} \approx (\sqrt{A_{FF}} - \sqrt{A_{WW}})^2 \quad (7)$$

where A_{FF} and A_{WW} are the Hamaker constants of fullerene nanoparticles and water interacting in a vacuum, respectively, and assuming $A_{WW} = 3.7 \times 10^{-20}$ J,⁵⁶ we calculate A_{FF} to be 7.5×10^{-20} J. Interestingly, this value is approximately 1 order of magnitude smaller than the Hamaker constants commonly assumed for carbon nanotubes in a vacuum or air ($2.3\text{--}6.0 \times 10^{-19}$ J).^{57–60}

3.4. Deposition Kinetics with Sodium and Calcium Cations.

Figure 5 presents representative normalized frequency shifts at the third overtone (Δf_3) as deposition takes place in the presence of 1, 10, and 30 mM NaCl onto a silica surface, and under favorable (fast) deposition conditions onto a PLL-coated silica surface in 1 mM NaCl. The mass of nanoparticles deposited onto the surface is proportional to the frequency shift as described by eq 3. Thus, the increase in the magnitude of frequency shift with time indicates that nanoparticles deposit as time progresses. Since this study focuses on the early stage deposition kinetics, the initial slopes are employed to derive the deposition attachment efficiency, α_D , from eq 4. Linear normalized frequency shift versus time curves were observed in most cases, except at high NaCl concentrations as discussed later.

The deposition kinetics of fullerene nanoparticles were examined over NaCl concentrations ranging from 1 to 300 mM and CaCl₂ concentrations ranging from 0.1 to 1.0 mM. Figure 6 presents the deposition attachment efficiencies, α_D , as functions of NaCl and CaCl₂ concentrations. Within the concentration ranges of 1–30 mM NaCl and 0.1–1.0 mM CaCl₂, as the electrolyte concentration increases, there is a corresponding increase in the deposition kinetics. The critical deposition concentrations (CDC) at which the attachment efficiencies α_D approach 1 are close to 30 mM NaCl and 0.6 mM CaCl₂. This deposition behavior is consistent with the DLVO theory. An

(49) Hogg, R.; Healy, T. W.; Fuerstenau, D. W. *Trans. Faraday Soc.* **1966**, 62 (522P), 1638–1651.

(50) Wiese, G. R.; Healy, T. W. *Trans. Faraday Soc.* **1970**, 66, 490–500.

(51) Usui, S. *J. Colloid Interface Sci.* **1973**, 44 (1), 107–113.

(52) Ottewill, R. H.; Shaw, J. N. *J. Electroanal. Chem.* **1972**, 37 (JUN), 133–142.

(53) Hunter, R. J. *Foundations of Colloid Science*; Oxford University Press: Oxford, U.K., 2002.

(54) Behrens, S. H.; Christl, D. I.; Emmerzael, R.; Schurtenberger, P.; Borkovec, M. *Langmuir* **2000**, 16 (6), 2566–2575.

(55) Kihira, H.; Matijević, E. *Langmuir* **1992**, 8 (12), 2855–2862.

(56) Israelachvili, J. *Intermolecular and Surface Forces*; Academic Press: London, 1991.

(57) Wang, G. W.; Zhang, Y.; Zhao, Y. P.; Yang, G. T. *J. Micromech. Microeng.* **2004**, 14 (8), 1119–1125.

(58) Akita, S.; Nishijima, H.; Nakayama, Y. *J. Phys. (Paris) D Appl. Phys.* **2000**, 33 (21), 2673–2677.

(59) Akita, S.; Nakayama, Y.; Mizooka, S.; Takano, Y.; Okawa, T.; Miyatake, Y.; Yamanaka, S.; Tsuji, M.; Nosaka, T. *Appl. Phys. Lett.* **2001**, 79 (11), 1691–1693.

(60) Snow, E. S.; Campbell, P. M.; Novak, J. P. *J. Vac. Sci. Technol. B* **2002**, 20 (3), 822–827.

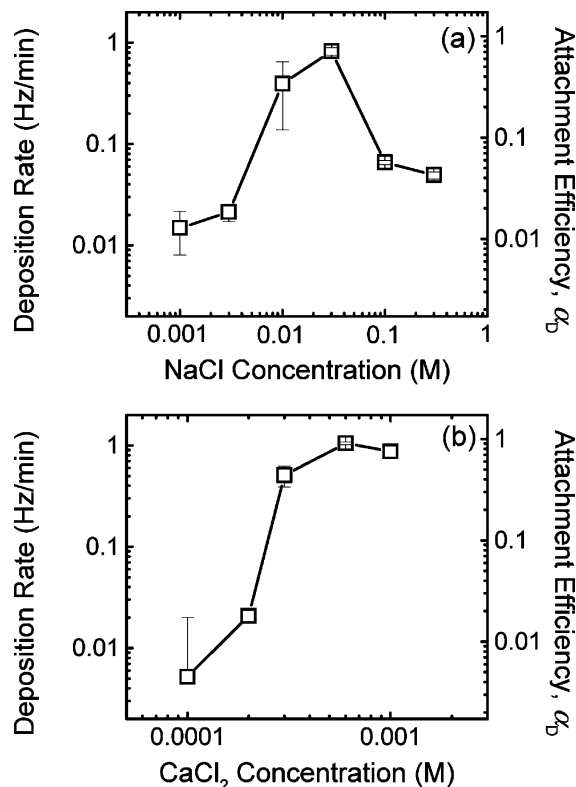


Figure 6. Deposition rates and attachment efficiencies onto a silica-coated quartz surface as functions of (a) NaCl and (b) CaCl₂ concentrations at pH 5.2. Deposition rates are expressed as the rates of normalized frequency shift at the third overtone. Each data point represents the mean of duplicate or triplicate measurements conducted at the same experimental conditions, and the error bars represent standard deviations.

increase in the monovalent and divalent electrolyte concentrations leads to a greater reduction of the energy barrier between the nanoparticles and the silica surface, which allows for a higher deposition rate. Toward the CDC, the energy barrier to deposition is almost eliminated as most of the electrostatic repulsive forces are suppressed. In such situations, the deposition kinetics are similar to those in which the fullerene nanoparticles are deposited onto an oppositely charged PLL-coated silica surface (i.e., $\alpha_D \approx 1$).

At the higher concentration range of NaCl (100–300 mM), the attachment efficiencies decrease significantly by an order of magnitude (Figure 6a). We have found the CCC of the fullerene nanoparticles to be 120 mM NaCl in the previous section. Thus, during the deposition process at NaCl concentrations close to or higher than the CCC, particle aggregation took place simultaneously with deposition. Since the aggregation was close to or within the diffusion-limited regime under such solution conditions, significantly large aggregate formation may occur in a relatively short period of time. This fast aggregate formation drastically decreased the diffusion coefficient of the nanoparticles and thus led to a decline in convective-diffusive transport of the fullerene nanoparticles/aggregates toward the silica-coated quartz surface.

A representative normalized frequency shift at the third overtone, $\Delta f_{(3)}$, is presented in Figure 7 as deposition takes place at 100 mM NaCl. The 100 mM NaCl electrolyte solution was flowed across the silica-coated quartz surface in the first 35 min, followed by the fullerene nanoparticle suspension in 100 mM NaCl. As deposition starts from 35 min onward, nonlinear deposition behavior is observed, where the rate of deposition decreases with time. This is indicative of aggregate growth as time progresses, which further decreases the rate of fullerene

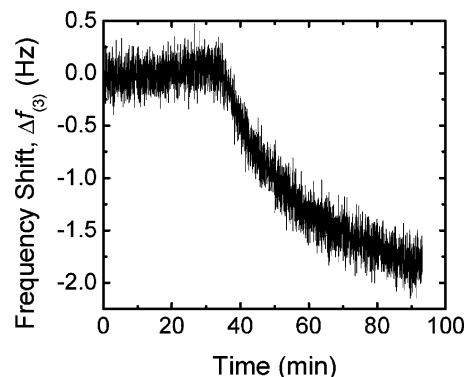


Figure 7. Nonlinear deposition behavior of fullerene nanoparticles onto a silica-coated quartz surface in the presence of 100 mM NaCl at pH 5.2. Deposition is indicated by the normalized frequency shift at the third overtone. The nonlinear deposition is attributed to simultaneous aggregation and deposition.

transport toward the silica surface. This nonlinear deposition behavior is observed in both 100 and 300 mM NaCl.

3.5. Release of Deposited Fullerene Nanoparticles upon Solution Chemistry Changes. In these experiments, the fullerene nanoparticles were first deposited onto the silica-coated quartz surface at electrolyte concentrations where nonrepulsive conditions prevail. Next, the solution chemistry of the flow over the deposited nanoparticles was altered to investigate the possibility of nanoparticle release from the surface. The flow rate was maintained at 0.1 mL/min throughout the experiments. In Figure 8, the pH of solutions introduced was kept constant at 5.2 from stages A to E. Solutions of 30 mM NaCl (Figure 8a) and 0.6 mM CaCl₂ (Figure 8b) were flowed across the silica surfaces in stage A. These electrolyte concentrations were chosen for $\alpha_D \approx 1$, as shown earlier. In stage B, the fullerene nanoparticles in the respective electrolyte solutions were directed across the silica surface to allow deposition to take place. The systems were then rinsed with the respective electrolyte solutions in stage C to flush away undeposited nanoparticles. In both systems, 1 mM NaCl electrolyte solutions followed by deionized water were flowed across the crystal surfaces in stages D and E, respectively. Although the range and magnitude of the electrostatic repulsive forces increased significantly as solution conditions were changed from 30 mM NaCl or 0.6 mM CaCl₂ to 1 mM NaCl and then to DI water, no significant release of the nanoparticles was observed, as indicated by the constant normalized frequency at the third overtone. There is a minor positive shift in the normalized frequency when the 30 mM NaCl electrolyte solution is displaced by 1 mM NaCl electrolyte solution (Figure 8a). This is due to the slight decrease in solution viscosity or density, which leads to a positive shift in frequency.⁶¹ This change in the normalized frequency is hardly noticeable when 0.6 mM CaCl₂ is displaced by 1 mM NaCl.

In stage F, deionized water with a pH adjusted to 12.3 (using NaOH) was flowed across the silica surface, and an immediate positive shift in the normalized frequency was observed in both systems. In a separate control test (results not shown), 30 mM NaCl (pH 5.2), deionized water at pH 5.2, and deionized water at pH 12.3 (adjusted with NaOH) were flowed across the crystal. Our results showed that the normalized frequency had a positive shift with the introduction of deionized water at pH 5.2, and then a negative shift of approximately 5 times the magnitude of the previous positive shift with the introduction of deionized water at pH 12.3. This negative shift was likely a result of the increase

(61) Martin, S. J.; Granstaff, V. E.; Frye, G. C. *Anal. Chem.* **1991**, 63 (20), 2272–2281.

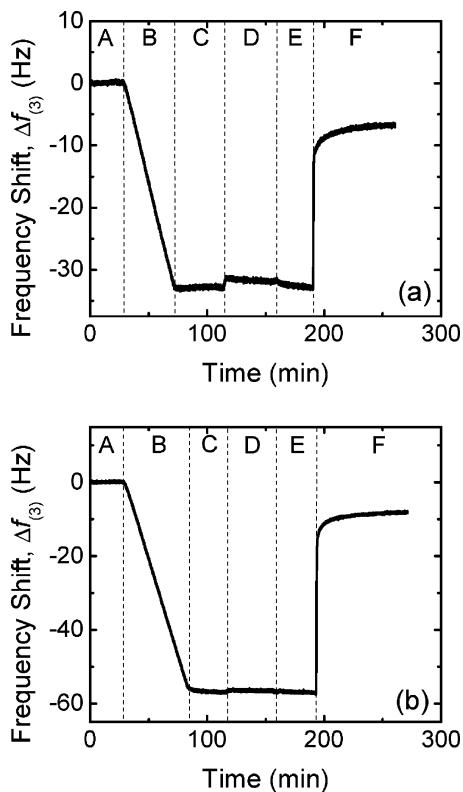


Figure 8. Fullerene nanoparticles are first deposited onto a silica-coated quartz surface in the presence of (a) 30 mM NaCl and (b) 0.6 mM $CaCl_2$ at pH 5.2, before being released by flushing with deionized water adjusted to pH 12.3. Baseline is first collected in the respective electrolytes (A), before the nanoparticles are deposited onto the quartz surface (B). The system is then rinsed in the respective electrolytes (C), 1 mM NaCl at pH 5.2 (D), deionized water at pH 5.2 (E), and finally, deionized water adjusted to pH 12.3 (F), where the release takes place.

in viscosity/density of the solution due to NaOH addition for pH adjustment. This test verifies that the sudden and significant positive shift in the normalized frequency in stage F was not due to changes in the physical properties of the solution, but rather due to the release of the deposited fullerene nanoparticles. However, because of the combined opposite effects, it is difficult to quantify the amount of nanoparticles released. Even though the range and magnitude of the electrostatic repulsive forces had

increased when 1 mM NaCl and deionized water were introduced (stages D and E), the deposited nanoparticles still remained in the primary energy minimum. However, once deionized water adjusted to pH 12.3 was introduced, it is likely that the marked increase in the surface potential of either the fullerene nanoparticles or the silica surface, or both, was sufficient to displace the nanoparticles out of the primary minimum, thus causing the release of the nanoparticles.

4. Conclusion

The aggregation and deposition kinetics of fullerene nanoparticles in the presence of monovalent and divalent electrolytes have been investigated. One important aspect of our study was to examine whether the classic DLVO theory for colloidal stability can be used to describe the aggregation and deposition behaviors of these emerging nanoparticles. Despite the uncertainty with regard to the origin of surface charge of the fullerene nanoparticles, it appears that electrostatic double layer repulsion controls their aggregation and deposition kinetics as predicted by the DLVO theory. Electrophoretic mobility of the particles became less negative as the electrolyte concentrations were increased, with divalent cations being more effective than monovalent cations. In the presence of NaCl and $CaCl_2$ electrolytes, an increase in the electrolyte concentrations resulted in a monotonic increase in the rate of aggregation until their respective CCC were reached. Above the CCC, aggregation occurred at the same maximum rate in both electrolytes, confirming diffusion-controlled aggregation kinetics. The significance of the role of electrostatic double layer repulsion of fullerene nanoparticles again manifested through the increase in their rate of deposition onto a negatively charged silica surface with increasing electrolyte concentrations. However, at electrolyte concentrations above the CCC, significant aggregate formation took place, thus reducing the convective-diffusive transport of the fullerene toward the silica surface. The deposition of fullerene nanoparticles onto the silica surface was mostly irreversible, with release only possible at extremely high pH conditions.

Acknowledgment. Funding was provided by the National Science Foundation (BES 0504258). We acknowledge Dr. Marc Pypaert (Department of Cell Biology, Yale University School of Medicine) for taking the TEM images in this study. We thank Q-Sense for kindly loaning us the E4 setup.

LA062072V